Predictive Analysis for Safe and Optimal Operation of the CoBra High-Temperature Heat Pump

Jina Yoo[1], Saskia Bublitz[2]

[1,2] *Institute of Low Carbon Industrial Processes, German Aerospace Center, Cottbus, Germany*
jina.yoo@dlr.de
saskia.bublitz@dlr.de

ABSTRACT

High-temperature heat pumps are a key technology enabling the decarbonization of conventional heating processes. The CoBra (Cottbus Brayton) high-temperature heat pump is a novel pilot plant, based on the reverse Brayton cycle, developed within DLR which achieves desired temperatures of more than 250 °C. However, during experiments, the pilot CoBra could no longer operate properly once the temperature of hydraulic oil, which is required to lubricate the compressor, exceeded the safety-relevant temperature limit. Emergency shutdowns were triggered to prevent compressor and components failure. Notably, the oil temperature rise occurs within a few minutes and shows no clear prior indication. As a consequence, the experimental objectives could not be fulfilled. This study develops a predictive model for the compressor oil temperature based on historical experimental data such as operating pressure and compressor speed, using deep learning techniques. The model aims to provide operators with early warnings during experiments and to recommend appropriate countermeasures that can prevent system shutdowns. Furthermore, this work investigates long-term operational strategies for the CoBra under varying input conditions through dynamic simulation. The oil temperature prediction model and process simulation model are combined into a unified framework, and a dynamic optimization problem, with rolling horizon approach, is formulated to simultaneously address process performance and machinery safety constraints. IPOPT is selected as the solver for this optimization problem as a proof of concept. The proposed method enables safer and more efficient operation, improves cost efficiency and extends equipment lifetime.

1. INTRODUCTION

Fault Detection and Diagnosis (FDD) refers to (i) the timely recognition of an element's inability to perform its required function, (ii) localization, and (iii) root cause identification (CEN, 2010). Together, these capabilities form the foundation for maintaining system reliability and safety. In this context, indicators such as Mean Time Between Failures (MTBF), operational availability, and maintainability provide quantitative measures for evaluating reliability enhancement and maintenance cost efficiency (Friederich & Lazarova-Molnar, 2024).

Recent advances in machinery knowledge and growing adoption of artificial intelligence applications, have significantly improved the ability to detect fault at an early stage and prevent catastrophic failures (Hrncir & Hickenbottom, 2024) (B. Dowdeswell & MacDonell, 2020; Dhiraj Neupane & Aryal, 2024). However, fault detection alone is not sufficient, as appropriate counteractions should be taken to restore the system to normal operation and prevent fault escalation, a process known as fault management. In practice, fault management often relies on human intervention and decision-making. These decisions often depend heavily on individual technical knowledge, experience, and judgment, which introduce delays and inconsistencies. Counteractions must therefore be executed both correctly and in a timely manner, which remains a challenging task (Chang Tian, 2025).

These limitations motivate the need for fault management approaches that are more universal, efficient, timely, and ideally automated. In this context, informed decision-making plays a central role. Previous studies have explored decision support based on fault symptoms interpretation and counteraction mapping using statistical techniques (Chang Tian, 2025). Additionally, a maturity framework for data-driven maintenance decision support is presented, aiming to enable increasingly autonomous decision-making (Chris Rijsdijk, 2024).

As FDD technologies are applied across many domains (B. Dowdeswell & MacDonell, 2020), this work focuses on heat pump applications. In particular, High-Temperature Heat Pumps (HTHPs) play a crucial role in decarbonizing industrial heating. This device recovers waste heat and upgrades it to higher temperature through an electrified process. Grow-

ing interest in reducing fossil fuel reliance for heat generation and the availability of waste heat make HTHP an economically attractive solution (Walden et al., 2023). Major challenges in large-scale heat pumps operation occur in its built-in components: compressor, evaporator, and condenser due to several operational issues such as fouling, leakage of refrigerant, and excessive vibration. Undetected or unidentified faults can lead to reduced performance, downtime, and higher maintenance cost (J. J. Aguilera, 2022).

The Institute of Low-Carbon Industrial Processes at the German Aerospace Center (DLR) successfully commissioned the novel HTHP called CoBra (Cottbus Brayton) located in Cottbus, Germany, in May 2024. The system is capable of delivering process heat at temperature of up to 260 °C (Yücel et al., 2025). Previous work on the CoBra includes development of a dynamic simulation model of the CoBra with calibrated compressor maps (Tran & Stathopoulos, 2025), used for safe start-up operation (Johannes Oehler, 2022). The model was developed in Modelica and can be used to analyze the thermodynamic cycle of the CoBra heat pumps. Transient behaviors influenced by the control strategy are investigated in (Matteo Pettinari & Ferrari, 2024). In addition, a conceptual model for heat pump integration to an industrial power-to-heat system has been investigated. (Walden et al., 2023).

The current development continues to expand the CoBra operating range toward more extreme conditions e.g. higher delivered temperature, higher compressor speed, higher pressure ratio. However, during certain experiments, excessively high compressor lubricating oil temperatures were observed, triggering emergency shutdowns and preventing the fulfillment of the test objectives. An anomaly detection and EXplainable Artificial Intelligence (xAI) framework has been developed for the CoBra based on emergency shutdown events (Lambert & Singh, 2025). However, the applied xAI methods do not establish causal relationships, thereby limiting the identification of effective countermeasures.

1.1. Goal of this paper

The goals of this study are:

1. To support informed operational decisions by developing a forecasting model for the oil system that predicts the oil temperature trajectory during load changes or compressor parameter variations
2. To enable automatic counteraction by dynamic optimization for long-term operational strategy of the CoBra system under realistic disturbances within safety constraints using a simulation-based approach.

1.2. Outline of this paper

The remainder of this paper is structured as follows. Section 2 introduces the CoBra system and describes the oil temperature problem. Section 3 presents the data pre-processing steps and prediction model selection. Section 4 reports the prediction model results and their evaluation. Section 5 introduces the CoBra model, the integration concept, and the optimization formulation, along with preliminary results. Finally, Section 6 concludes the paper and provides an outlook for future work.

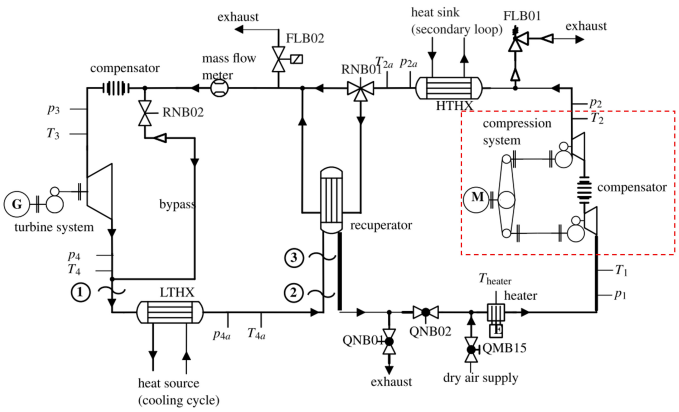

Figure 1. P&ID of the CoBra heat pump (Yücel et al., 2025)

2. THE COBRA HIGH-TEMPERATURE HEAT PUMPS

The CoBra HTHP is based on a reversed Brayton cycle using dry air as the working medium. The HTHP consists of two compressors: ASA520 (first stage) and ASA316 (second stage), three shell-and-tube heat exchangers: condenser, evaporator, and recuperator, and one turbine, which are connected in closed-loop configurations. Fig. 1 shows the P&ID of the CoBra demonstrator, with the focus of this paper on the compression system marked by the red dashed line. Further descriptions of the test rig are provided in (Yücel et al., 2025; Tran & Stathopoulos, 2025).

2.1. Oil system descriptions

In the CoBra system, the two compressors and the turbine are equipped with separate lubrication systems. This study considers only the lubrication system of the compressors. The compressor lubrication system, referred to as Hydrobar, consists of an oil reservoir with a capacity of 70 L, an electric motor and pump, an oil cooler, pipe fittings, hydraulic hoses, and other connecting components as shown in Fig. 2. The maximum allowable oil temperature in the reservoir before system startup is limited to 50 °C. During operation, the oil pump supplies oil to both compressors for lubrication, and the return oil flows through a cooling unit before being stored back in the reservoir. According to the manufacturer's manual, the required oil flow rate per compressor is specified to be between 1.2 and 1.6 litre per minute. Several manufacturers specify an effective operating temperature for compressor seals and bearings in the range of 100–120 °C, depending on their materials and designs (Wong, 2025; SKF, 2025). There-

fore, oil temperatures exceeding this range are considered unsafe, as they may deteriorate these components.

2.2. Problem descriptions

The CoBra test rig was developed as a proof-of-concept for a closed-loop Brayton high-temperature heat pump (HTHP). The system is designed for scalable on-site industrial integration and to deliver high-temperature heat beyond currently available solutions. The present operational limit reaches a maximum temperature of 260 °C; further development aims to extend this range to higher delivery temperatures and more extreme operating conditions. Under certain extreme conditions, such as low inlet pressure or high compressor speed, the oil temperature exceeds 110°C within a few minutes, triggering an emergency shutdown. Figures 3 illustrate the compressor maps for the first and second compression stages, with the speed lines corresponding to percentages of the maximum speed. $Phic$ refers to the corrected mass flow rate, expressed in Eq. (4). The grey markers represent operating points from all conducted tests, while the red markers indicate operating points at which oil temperatures exceeding 100 °C were observed.

Preliminary observations depicted in Fig. 4 and 5 indicate that T_{oil1} varies inversely with compressor inlet pressure and increases proportionally with speed. Nevertheless, it is important to understand how these parameters affect oil temperature rise and to identify the operating conditions that ensure safe and reliable performance.

3. METHODOLOGY

This section describes the data processing steps used to prepare the input data for developing a prediction model for the temperatures at T_{oil1} (BTB038) and T_{oil2} (BTB039).

3.1. Data descriptions

The experimental data is publicly available via (Center, 2025). Each test stored in an individual csv file and contains multiple sensor measurements from tests made during 2024 to 2025. All datasets have a 1-Hz sampling frequency. In total, the dataset comprises 130.5 hours of measurement data from CoBra operation. For the detailed P&ID with sensor locations, please refer to the cited reference.

3.2. Data Pre-Processing and Feature Engineering

1. Data Cleaning and Missing Values Handling

Measurements recorded during plant standby and start-up periods are removed, as the sensor readings are highly noisy and irrelevant. Missing values are handled in Python using the Pandas functions backward fill *bfill()* followed by forward fill *ffill()* (Wes McKinney, 2010). Columns containing only NaN values are replaced with zeros.

Table 1. Selected sensor list

Sensor ID	Sensor descriptions
BPB002	Outlet pressure at the 2nd compressor
BPB022	Inlet pressure at the 1st compressor
BPB059	Inlet pressure at the 2nd compressor
BPB100	Outlet pressure at oil supply line
BTB013	Inlet temperature at the 1st compressor
BTB038	Oil return temperature at the 1st compressor, T_{oil1}
BTB039	Oil return temperature at the 2nd compressor, T_{oil2}
BTB056	Oil temperature in the tank
BGD001	Rotational speed of the 1st compressor
BFB001	Inlet mass flow rate of the 1st compressor

2. Feature Selection

This dataset exhibits temporal dependencies as the current measurements depend on past values, but the time at which tests are conducted is insignificant. No ambient or seasonal influences are recognized as all tests are conducted indoor in a controlled environment. Therefore, the features corresponding date and time are removed. Compressor- and oil- sensor features were selected, while sensor measurements from downstream components were removed for a compact model. The selected features are listed in Table 1, comprising a total of ten input features.

3. Data Distribution

Feature distribution analysis was conducted to ensure coverage of the full operating range. As shown in Fig. 6, high oil temperature events are significantly underrepresented, with the majority of samples concentrated in the normal operating range (60–80 °C) for both T_{oil1} and T_{oil2}, indicating a clear data imbalance. Adequate representation of rare events is essential to ensure reliable model performance in this extreme range. Therefore, resampling techniques were applied by duplicating rare event samples ten times and computing a different moving average across the ten duplicated datasets. The purpose is to improve prediction accuracy under high-temperature conditions.

4. Data Normalization

All datasets are concatenated into a single data frame and scaled simultaneously using Min-Max scaler expressed in Eq. (1). Then, the data are spitted back into their original dataset lengths.

$$X_{scaled} = \frac{X - X_{min}}{X_{max} - X_{min}} \tag{1}$$

where X is the original value, X_{min} and X_{max} are minimum and maximum values of the selected feature.

5. Time Series Forecasting (TSF)

To generate lagged data for forecasting, two data configurations are applied: Single-Step Forecasting and Sequence-to-

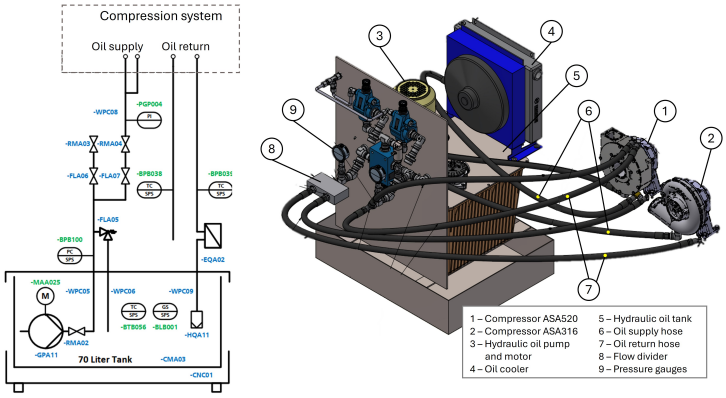

Figure 2. Oil system connection: Schematic diagram (left) and 3D drawing with component descriptions (right)

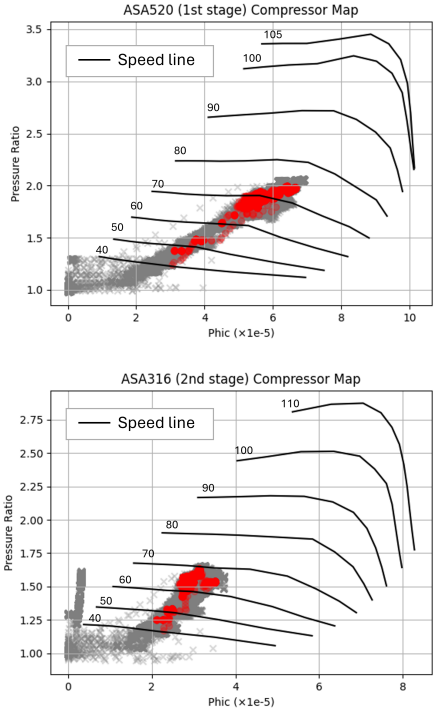

Figure 3. Compressor maps: first and second stages

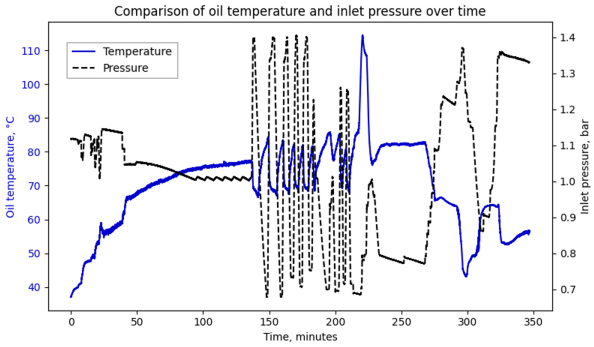

Figure 4. T_{oil1} changes under fluctuating pressure

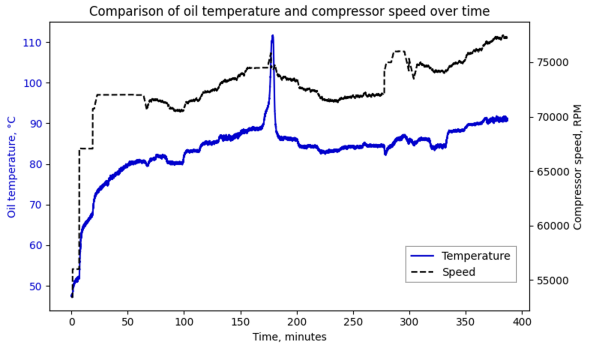

Figure 5. T_{oil1} changes under increased speed

Sequence Forecasting (Mariet & Kuznetsov, 2019). The selection of the configuration depends on the model selection described in Section 3.3.

In the Single-Step Forecasting setup, input features at current time step $\mathbf{X}_t$ are used to predict the temperatures T_{oil1} and T_{oil2} at the next 15-minute (900 s), $\hat{\mathbf{y}}_{t+900}$.

In the Sequence-to-Sequence Forecasting, a 15-minute look-back window of selected input features is used to predict the temperatures T_{oil1} and T_{oil2} over the next 15-minute forecasting horizon. A stride, or a number of samples skipped to move to the next consecutive window, is set to 5 minutes, creating overlapping sequences and thereby increasing the number of training samples. Padding techniques are applied to prevent data loss during transformation.

3.3. Forecasting model

The evaluated models selected for this study are categorized into tree-based models and deep neural network architectures, chosen to evaluate the trade-offs between computational efficiency, generalization, and the ability to capture temporal dynamics. Tree-based methods include Random Forest (RF), an ensemble of randomized decision trees that improves generalization, and Gradient Boosting Trees (GBT), which se-

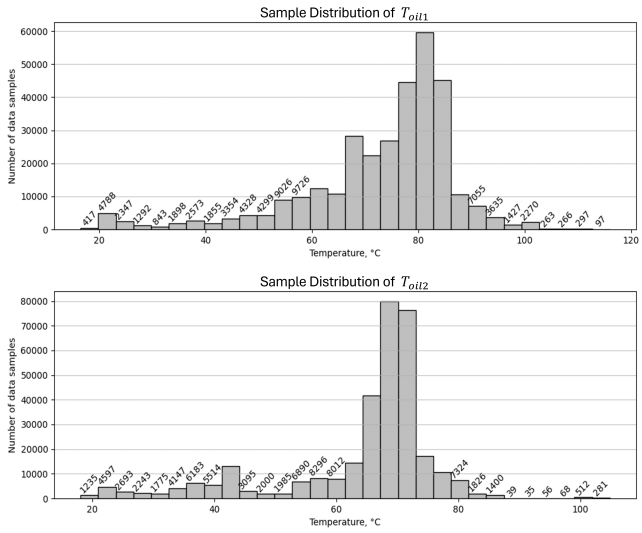

Figure 6. Data sample distribution across temperature, T_{oil1} (top), T_{oil2} (bottom)

quentially combine weak learners to enhance predictive accuracy (C. Bentéjac & Martínez-Muñoz, 2021). To address the temporal dependencies in the CoBra experimental data, deep learning approaches including Long Short-Term Memory (LSTM) and Temporal Convolutional Networks (TCN) were implemented. Long Short-Term Memory (LSTM) networks capture short- and long-term dependencies via gated memory cells, mitigating vanishing gradients (Zonglei Chen & Li, 2023), while Temporal Convolutional Networks (TCN) use dilated causal convolutions to efficiently model long-range sequences (Mehta & Yang, 2023). Furthermore, Artificial Neural Networks (ANNs) with fully-connected layers is included due to its simple analytical form and suitability for optimization problem integration described in Section 5.1. The algorithms RF, GBT, and ANNs are configured for single-step forecasting while LSTM and TCN use sequence-to-sequence forecasting, as discussed in Section 3.2.5.

4. PREDICTIVE MODEL RESULTS

For each algorithm, hyperparameter tuning is performed, and only the configuration achieving the highest R-squared is reported. The results shown are based on testing with the datasets *CoBra20250115* and *CoBra20250224*. Due to limited computational resources, all models are trained for a maximum of 500 epochs, and 500 number of estimators for tree-based models. The training was terminated when loss are saturated.

Figure 7 illustrates the predicted temperatures T_{oil1} and T_{oil2} from all models compared with the ground truth for the test dataset *CoBra20250115*. Furthermore, zoomed-in views of the T_{oil1} prediction results during three operation scenarios are shown: (i) the slow temperature rise after the start-up process (Fig. 8), (ii) periods of rapid temperature fluctuations (Fig. 9), and (iii) the high temperature rise observed in the

Table 2. Evaluation metrics

Algorithms	RMSE	R-Squared	Train time, s
RF	0.0654	0.6295	188
GBT	0.1026	0.3143	453
ANN	0.0704	0.6794	8923
LSTM	0.0577	0.7262	11345
TCN	0.0588	0.7090	6538

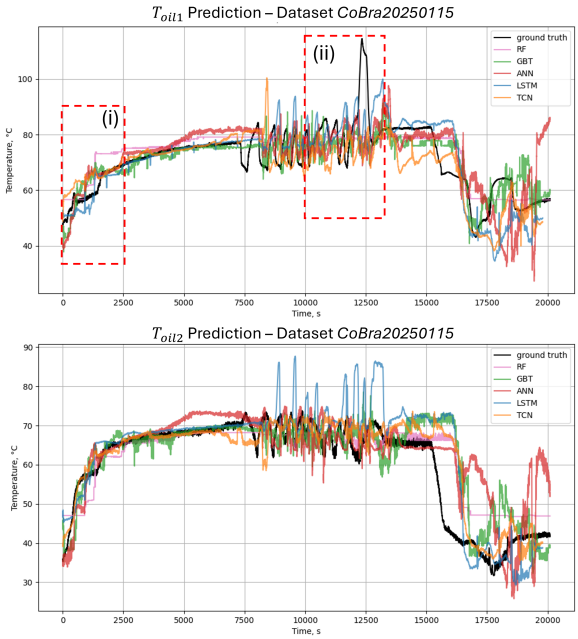

Figure 7. Predictions and ground truth comparison: Entire test set *CoBra20250115*, T_{oil1} (top), T_{oil2} (bottom)

test dataset *CoBra20250224*, for which the complete set of predictions is not shown (Fig. 10). Under condition (i), all models capture the overall trend during gradual temperature increases, although RF performs worst among the five compared models. However for condition (ii), the models struggle to reproduce short-term fluctuations and abrupt temperature changes, particularly at higher temperature levels. While the predicted temperatures generally follow the process variations, they exhibit a noticeable time lag. At condition (iii), only the LSTM model is capable of predicting temperatures above 90 °C, with a delayed response. None of the models accurately predict values exceeding 110 °C. In the author's view, the inability to predict at a high temperature range is due to the limited number of training samples in this range. As a result, the models are biased toward the more frequent lower-temperature data and show reduced generalization in the extreme range.

The performance metrics are reported in Table 2, including RMSE, R-Squared, and training time. The ANN achieved the highest R-squared for single-point forecasting, while LSTM achieved the highest R-squared for sequence-to-sequence fore-

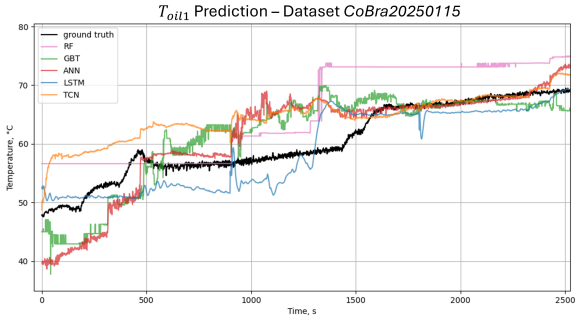

Figure 8. T_{oil1} Predictions and ground truth comparison: (i) under slow temperature rise

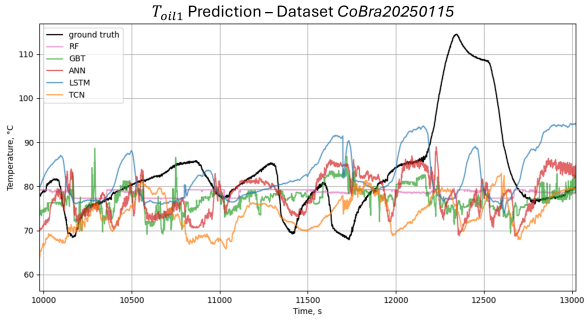

Figure 9. T_{oil1} Predictions and ground truth comparison: (ii) under temperature fluctuations

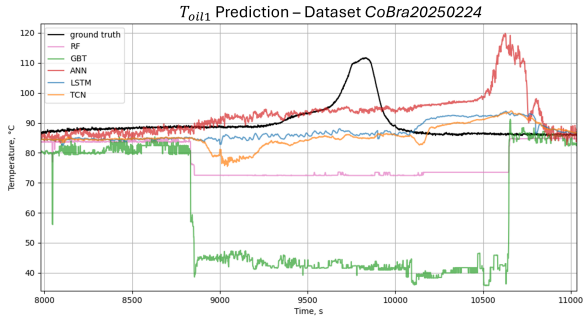

Figure 10. T_{oil1} Predictions and ground truth comparison: (iii) under high temperature rise

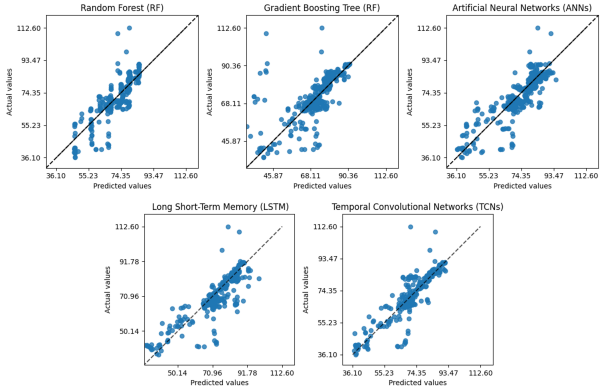

Figure 11. Parity plots

casting. However, the LSTM required the longest training time. To further analyze the model performance, the parity plots for each algorithm are shown in Fig. 11. For all algorithms, the smallest residuals occur in the 60–80 °C range where the training samples are abundant. On the other hand, high prediction errors appeared at temperature above 90°C, which corresponds to a fewer samples in this range.

5. CASE STUDY FOR OPERATIONAL OPTIMIZATION

The purpose of this case study is to develop a long-term operational optimization strategy for the CoBra system while accounting for short-term safety-relevant constraints, such as oil temperatures, predicted by the model described in Section 4. The investigation focuses on how short-term effects influence heat pump operation and evaluate their impact on operational cost, maintenance cycle, and equipment lifetime.

5.1. Model Level

A simplified simulation model of the CoBra system is developed. The calibrated compressor maps of the CoBra compressors (Tran & Stathopoulos, 2025) are reused in this work. For simplicity, the system configuration is reduced to an open-loop heat pump model, implemented in *Pyomo* (Bynum et al., 2021; Hart, Watson, & Woodruff, 2011). The integration concept is depicted in Fig. 12, comprising model level and optimization level. At the model level, the overall model consists of two components:

1. An open-loop heat pump model
2. A compressor oil temperature prediction model

The simplified open-loop heat pump model includes two radial compressors, a heat exchanger, and a turbine. The thermodynamic processes are modeled as isentropic compression, isobaric heat addition, and isentropic expansion. The only control input of the model is the rotational speed of the first compressor, N_1. The rotational speed of the second compressor is determined by Eq. (2), since both compressors are driven by the same motor but operate with different gear ratios.

$$N_2 = 1.05 \cdot N_1 \tag{2}$$

The system mass flow rate, $\dot{m}$, and the corrected mass flow, $Phic$, can be expressed in Eq. (3) and (4)

$$\dot{m} = \dot{m}_{nominal} \cdot \frac{N_1}{N_{nominal}} \tag{3}$$

$$Phic = \dot{m} \cdot \frac{\sqrt{T}}{P} \tag{4}$$

The compressor pressure ratio PR and efficiency η are ob-

tained from the compressor map, which are normalized and linearized, resulting in the following Eq. (5)-(8)

$$PR_1 = (-84.922 \cdot Phic + 0.0317) \cdot N_1 \quad (5)$$

$$\eta_1 = (-9.878 \cdot Phic + 0.0078) \cdot N_1 \quad (6)$$

$$PR_2 = (-95.195 \cdot Phic + 0.0268) \cdot N_2 \quad (7)$$

$$\eta_2 = (-14.539 \cdot Phic + 0.0081) \cdot N_2 \quad (8)$$

The remaining components are modeled according to the thermodynamic cycle described in (Yunus A. Cengel, 2025). The heat pump system is connected to three boundaries B1, B2, and B3, which represent the inlet of the heat pump, the outlet of the heat pump, and the inlet of the heat sink respectively, with following conditions

- B1: $T = 26.85°C, P = 200000 + 50000 \cdot sin(\frac{\Pi t}{12})Pa$
- B2: $T = 0°C$, free pressure boundary
- B3: $\dot{m} = 1kg/s, T = 15 + 100 \cdot sin(\frac{\Pi t}{12})°C$

The second part is an oil prediction model that derives from the approach presented in Section 4. The ANN model is selected because of its simple analytical form, which allows direct implementation in *Pyomo*. The network consists of an input layer, two hidden layers, and an output layer. The input vector $\mathbf{X}$, is obtained from the state variables from the heat pump model with the 10 features listed in Table 1. The output vector $\hat{\mathbf{y}}$, consists of the predicted oil temperatures T_{oil1} and T_{oil2}, for the next 15 minutes and can be calculated from Eq. (9)-(11).

$$\mathbf{h}_1 = \sigma\left(\mathbf{W}_1\mathbf{X} + \mathbf{b}_1\right) \quad (9)$$

$$\mathbf{h}_2 = \sigma\left(\mathbf{W}_2\mathbf{h}_1 + \mathbf{b}_2\right) \quad (10)$$

$$\hat{\mathbf{y}} = \left(\mathbf{W}_3\mathbf{h}_2 + \mathbf{b}_3\right) \quad (11)$$

where σ denotes the activation function, $\mathbf{h}_i$ represents the neuron at the *i-th* hidden layer. The weights $\mathbf{W}_i$ and biases $\mathbf{b}_i$ are obtained from the trained neural networks.

5.2. Optimization Level

At the optimization level from Fig 12, the goal of the operational optimization is to determine the decision variable, which are the compressor speed at different time steps, such that heat pump operates in a safe region, satisfies the required heat demand, and adapts under fluctuating source and sink conditions. The model output over each timestep will be used in the objective function, which is defined by.

$$\underset{\mathbf{N} \in S}{\text{minimize}} \quad \sum_{k=1}^{T} c_{elec} \cdot P_k(\mathbf{N}) + c_p \cdot g_k(\mathbf{N}) + c_{oil} \cdot f_k(\mathbf{N})$$

where $\mathbf{N}$ represents the input rotational speed, T is the number of time steps, P_k denotes the electrical power consumption of the compressors at the *k-th* timestep. The electricity cost is denoted by c_{elec}, fixed at 96 $Eur/(MW \cdot h)$ (Bundesnetzagentur, 2026). The term $g_k = (T_{supply,k} - T_{desired,k})^2$ is a penalty at the *k-th* timestep applied whenever the desired temperature could not be achieved. The term $f_k(x) = (T_{oil1,k} - T_{safety})^2$. $T_{oil1,k}$ is the predicted oil temperature at BTB038 at the *k-th* timestep, T_{safety} is the safety oil temperature limit which sets at 70°C. The coefficients c_p, and c_{oil} are weight factors for respective terms and are tuned to explore different optimization scenarios, as summarized in Table 3. Based on the historical data, T_{oil2} is also dependent on T_{oil1}. Therefore it was excluded from the objective function as the T_{oil1} sufficiently represents the compressors thermal constraint.

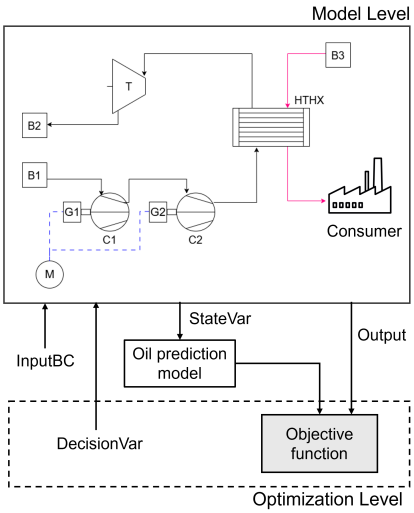

Figure 12. Integration concept: Model level and Optimization level

The optimization is performed using a rolling horizon approach (Kyriakidis, Kansara, & Roldán Serrano, 2025). The optimization horizon is set to 4 hours, with 1-hour segments and 15-minute step size. The total simulation period spans one week.

5.3. Optimization Results

The preliminary results of the optimization are presented in this subsection. Three optimization scenarios were solved using IPOPT (Wächter & Biegler, 2004) with the default linear solver MUMPS.

The first scenario is to give priority to safety constraint, the second is to prioritize the penalty constraint, and the third is to give equal priority to both safety and penalty constraint. This prioritization is performed by tuning the weight factor at each objective terms. The maximum iteration is set to 100. The optimization results including the objective values, total operating cost defined as $cost = \sum_{k=1}^{T} c_{elec} \cdot P_k(\mathbf{N})$, and

Table 3. Optimization results

	Values
Scenario 1: $c_p = 1, c_{oil} = 100$	
Objective	5.025×10^4
Operating cost, EUR	3010.64
CPU time, s	1.68
Scenario 2: $c_p = 100, c_{oil} = 1$	
Objective	3.81×10^3
Operating cost, EUR	3316.22
CPU time, s	1.86
Scenario 3: $c_p = 100, c_{oil} = 100$	
Objective	5.057×10^4
Operating cost, EUR	3316.22
CPU time, s	1.03

CPU time are reported in Table 3.

In scenario 1, the solutions ensure oil temperature safety and minimize operating cost. Therefore, the system operates at a relatively low cost, satisfying safety-related constraints but the delivered heat does not reach the desired temperature. In scenario 2, the solutions ensure that the supplied heat reaches the desired temperature, leading to an increase in the total operating cost compared to Scenario 1. In scenario 3, both safety and heat quality are equally prioritized. Under these conditions, the system likely has a physical trade-off between heat delivery and oil safety. This result highlights a limitation of the current objective formulation that the maintenance cost from unsafe operation are not explicitly incorporated into the total operating cost. Therefore, this objective formulation needs to be improved. The computational times for all cases are similar, with less than two seconds to solve. This CPU time validates the feasibility of the real-time fault management, as rapid execution enables automated responses to anomalies in heat pump systems.

6. CONCLUSIONS AND OUTLOOK

6.1. Conclusions

This study is the first to systematically analyze the unreliable operating conditions observed in CoBra, with particular focus on the oil temperature issue. The data profiles and distributions were examined, and data-driven predictive models for oil temperature were developed and compared. These models aim to support operational decision-making and provide early warnings prior to unsafe operating conditions. Furthermore, an integration concept linking the CoBra thermodynamic system with the oil temperature prediction in machinery was implemented through simulation. An operational optimization was then performed, considering external fluctuations, avoiding unsafe operation, and optimal cost efficiency. The results give prospects to extension to a better formulated optimization problem on safety-relevant constraints that would help minimizing equipment downtime and maintenance costs.

6.2. Outlook

The next phase of this study focuses on improving the prediction accuracy of the oil temperature for operating conditions above 90°C, which can be achieved through additional data augmentation, the integration of new experimental data collected in 2026, and adoption of Physics-Informed Neural Networks (PINNs) (X. Pan & Wang, 2024). The model will then be integrated with LabVIEW via OPC UA for online testing. In this configuration, measurement data will be continuously collected and real-time predictions will be generated during operation, enabling operators to monitor the system and maintain CoBra within a safe operating region.

Regarding the integration concept, the next step is to extend the optimization framework to a higher-fidelity closed-loop heat pump model developed in the Modelica environment. An initial integration using the Functional Mock-up Unit (FMU) approach was tested but resulted in long computational times. Therefore, Modelica2Pyomo (De Pascali, Biegler, Martelli, & Casella, 2025) is considered a promising alternative. For the optimization study, the objective function will be reformulated to incorporate maintenance costs, with the aim of minimizing downtime and improving cost efficiency. Furthermore, a systematic sensitivity analysis will be conducted to better understand the trade-offs between oil safety, operational cost, and maintenance cost priorities.

REFERENCES

B. Dowdeswell, R. S., & MacDonell, S. G. (2020). Finding faults: A scoping study of fault diagnostics for industrial cyber–physical systems. *J. Syst. Softw.*, *vol. 168, 110638*.

Bundesnetzagentur. (2026). Market data visuals: Electricity generation. *SMARD.de*. Retrieved from `https://www.smard.de/en/`

Bynum, M. L., Hackebeil, G. A., Hart, W. E., Laird, C. D., Nicholson, B. L., Siirola, J. D., ... Woodruff, D. L. (2021). *Pyomo–optimization modeling in python* (Third ed., Vol. 67). Springer Science & Business Media.

C. Bentéjac, A. C., & Martínez-Muñoz, G. (2021). A comparative analysis of gradient boosting algorithms. *Artificial Intelligence Review*, *54*, 1937-1967.

CEN. (2010). *En 13306: Maintenance - maintenance terminology.* European Committee for Standardization (CEN).

Center, G. A. (2025). Cobra high temperature heat pump demonstrator - experimental dataset 2024-2025. *Zenodo*. Retrieved from `https://zenodo.org/records/15862451` doi: 10.82481/cobra.2025

Chang Tian, F. Y. H. F. X. G., Pengcheng Gao. (2025). A knowledge transfer-based intelligent decision support

method for fault management. *Journal of Process Control*, *151*, 103452.

Chris Rijsdijk, T. T., M.J.R. van de Wijnckel. (2024). A maturity framework for data driven maintenance. In *Proceedings of the 8th european conference of the prognostics and health management society* (Vol. ISBN – 978-1-936263-40-0). PHM Society.

De Pascali, M., Biegler, L., Martelli, E., & Casella, F. (2025, 10). Modelica2pyomo: a tool to translate modelica models into pyomo optimization models. In *Modelica conferences.* doi: 10.3384/ecp218117

Dhiraj Neupane, R. D., Mohamed Reda Bouadjenek, & Aryal, S. (2024). A comparative study of semi-supervised anomaly detection methods for machine fault detection. In *Proceedings of the 8th european conference of the prognostics and health management society 2024* (Vol. ISBN – 978-1-936263-40-0). PHM Society.

Friederich, J., & Lazarova-Molnar, S. (2024). Reliability assessment of manufacturing systems: A comprehensive overview, challenges and opportunities. *Journal of Manufacturing Systems*, *72*, 38-58. doi: https://doi.org/10.1016/j.jmsy.2023.11.001

Hart, W. E., Watson, J.-P., & Woodruff, D. L. (2011). Pyomo: modeling and solving mathematical programs in python. *Mathematical Programming Computation*, *3*(3), 219–260.

Hrncir, Z., & Hickenbottom, C. (2024). A practical example of applying machine learning to a real turbofan engine issue: Neop. In *Proceedings of the 8th european conference of the prognostics and health management society* (Vol. ISBN – 978-1-936263-40-0). PHM Society.

J. J. Aguilera, T. O. W. B. M. J. L. P. e. a., W. Meesenburg. (2022). A review of common faults in large-scale heat pumps. *Renew. Sustain. Energy*, *vol. 168, 112826*.

Johannes Oehler, P. S., A. Phong Tran. (2022). Simulation of a safe start-up maneuver for a brayton heat pump. In *Proceedings of asme turbo expo 2022 turbomachinery technical conference and exposition* (Vol. GT2022, p. V004T06A003). ASME.

Kyriakidis, L., Kansara, R., & Roldán Serrano, M. I. (2025). Energy management of industrial energy systems via rolling horizon and hybrid optimization: A real-plant application in germany. *Energies*, *18*(15). doi: 10.3390/en18153977

Lambert, B., & Singh, D. (2025). Investigating explainable ai enhanced anomaly detection methods for emergency shutdown mitigation in high-temperature heat pump. In *2025 the 9th international conference on system reliability and safety.*

Mariet, Z., & Kuznetsov, V. (2019). Foundations of sequence-to-sequence modeling for time series. In *Proceedings of the 22nd international conference on artificial intelligence and statistics (aistats)* (Vol. ISBN – 978-1-936263-40-0, p. 89).

Matteo Pettinari, A. P. T. J. O. P. S. K. K., Guido Francesco Frate, & Ferrari, L. (2024). Impact of the regulation strategy on the transient behavior of a brayton heat pump. *Energies*, *17, 1020*.

Mehta, A., & Yang, W. (2023, December). Nac-tcn: Temporal convolutional networks with causal dilated neighborhood attention for emotion understanding. In *Proceedings of the 2023 7th international conference on video and image processing.* ACM. doi: 10.1145/3639390.3639392

SKF. (2025). Temperature limits: Rolling element bearings. *SKF*. Retrieved from `https://www.skf.com/group/products/`

Tran, A. P., & Stathopoulos, P. (2025). Dynamic simulation and experimental validation of a high-temperature brayton heat pump. *Applied Thermal Engineering*, *274*, 126536. doi: https://doi.org/10.1016/j.applthermaleng.2025.126536

Walden, J. V., Bähr, M., Glade, A., Gollasch, J., Tran, A. P., & Lorenz, T. (2023). Nonlinear operational optimization of an industrial power-to-heat system with a high temperature heat pump, a thermal energy storage and wind energy. *Applied Energy*, *344*, 121247. doi: https://doi.org/10.1016/j.apenergy.2023.121247

Wes McKinney. (2010). Data Structures for Statistical Computing in Python. In Stéfan van der Walt & Jarrod Millman (Eds.), *Proceedings of the 9th Python in Science Conference* (p. 56 - 61). doi: 10.25080/Majora-92bf1922-00a

Wong, P. (2025). Understanding bearing temperature limits. *EGI Blog*. Retrieved from `https://egibearing.com/`

Wächter, A., & Biegler, L. T. (2004). On the implementation of an interior-point filter line-search algorithm for large-scale nonlinear programming. *Mathematical Programming 106(1)*, *25-57*.

X. Pan, Y. J. Z. C., K. Liang, & Wang, Y. (2024). Interpretable chiller fault diagnosis based on physics-guided neural networks. *J. Build. Eng.*, *86*.

Yunus A. Cengel, M. K., Michael A. Boles (Ed.). (2025). *Thermodynamics: An engineering approach 10e*. McGrawHill.

Yücel, F. C., Oehler, J., Kriese, M., Jende, E., Setzepfand, N., & Stathopoulos, P. (2025). Design, commissioning and closed-loop operation of a high-temperature brayton heat pump — cobra. *Applied Thermal Engineering*, *279*, 127947. doi: https://doi.org/10.1016/j.applthermaleng.2025.127947

Zonglei Chen, T. L. H. W., Minbo Ma, & Li, C. (2023). Long sequence time-series forecasting with deep learning: A survey. *Information Fusion*, *97*.